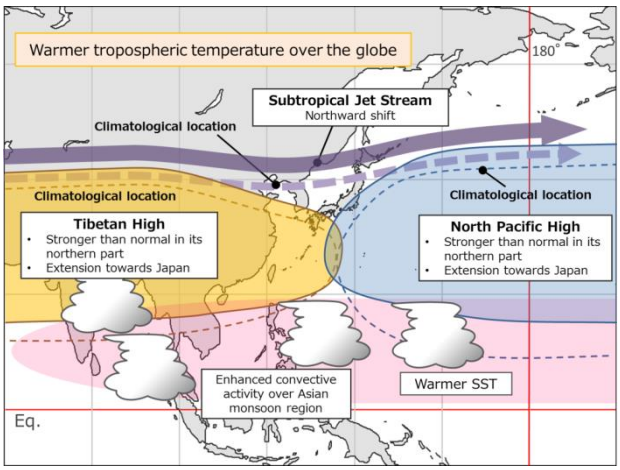

Figure 10: Conceptual diagram showing expected large-scale ocean/atmosphere characteristics for summer 2018

Summary of the 2017/2018 Asian Winter Monsoon

This report summarizes the characteristics of the surface climate and atmospheric/oceanographic considerations related to the Asian winter monsoon for 2017/2018.

Note: The Japanese 55-year Reanalysis (JRA-55; Kobayashi et al. 2015) atmospheric circulation data and COBE-SST (Ishii et al. 2005) sea surface temperature (SST) data were used for this investigation. The outgoing longwave radiation (OLR) data referenced to infer tropical convective activity were originally provided by NOAA. The base period for the normal is 1981 – 2010. The term "anomaly" as used in this report refers to deviation from the normal.

1. Surface climate conditions

Temperature anomalies in Asia for boreal winter 2017/2018 were generally high both north of 60°N and south of 30°N, and were low in the latitudinal band between 30 and 60°N (Figure 11). In particular, the eastern part of East Asia experienced lower-than-normal temperatures as often observed in La Niña winters. Three-month mean temperatures for December 2017 to February 2018 were extremely high from eastern to central parts of Eastern Siberia and in the northern part of Western Siberia. Precipitation amounts during this period were above normal in Southeast Asia and from the western part of Eastern Siberia to Central Siberia, and were below normal from eastern to southern parts of East Asia and in and around India (Figure 12). The wetter-than-normal conditions observed in Southeast Asia were consistent with typical anomaly patterns observed in past La Niña events. Three-month mean precipitation amounts for December 2017 to February 2018 were extremely high in and around southern Central Siberia.

Figure 13 shows extreme climate conditions observed between December 2017 and February 2018. In December, extremely high temperatures were seen in the northeastern part of Eastern Siberia and in and around southwestern China. Extremely high precipitation amounts were observed from the southern part of Central Siberia to northwestern Mongolia.

In January, extremely high temperatures were seen in the eastern part of Eastern Siberia, and extremely low temperatures were seen from central Mongolia to eastern Kazakhstan. Extremely high precipitation amounts were observed in and around the central part of the Philippines, the southern Malay Peninsula and central Mongolia, while extremely low precipitation amounts were observed in and around the southeastern part of Central Asia. In February, extremely high temperatures were seen in Eastern Siberia and in and around the northeastern part of Southeast Asia.

2. Characteristic atmospheric circulation and oceanographic conditions

2.1 Conditions in the tropics

The La Niña conditions that emerged in boreal autumn 2017 matured in winter 2017/2018. Remarkably positive SST anomalies were observed in the western equatorial Pacific and negative SST anomalies were observed from central to eastern parts of the equatorial Pacific (Figure 14), as often seen during La Niña events.

An active convection phase of the Madden-Julian Oscillation (MJO) propagated eastward from the Indian Ocean to the Maritime Continent in January (Figure 15). Convective activity inferred from OLR during this period was enhanced from the Indochina Peninsula to the seas east of the Philippines and was suppressed over the equatorial Indian Ocean and from the west of the date line to the central equatorial Pacific (Figure 16 (a)), which is also typical of La Niña episodes. Over the Maritime Continent, convective activity was enhanced in January (Figure 16 (c)), and weakened in February in association with eastward propagation of the MJO phase (Figure 16 (d)).

In the upper troposphere, clear large-scale divergent anomalies were seen over the western Pacific in association with enhanced convective activity, and convergent anomalies were observed over the Middle East (Figure 17 (a)). In the 200-hPa stream function field, a wave train stretched from Northern Africa to the northern part of East Asia with anti-cyclonic circulation anomalies extending from eastern India to southern China (Figure 17 (b)).

In the lower troposphere, cyclonic circulation anomalies straddling the equator were seen from the Indian Ocean to the Maritime Continent (Figure 17 (c)).

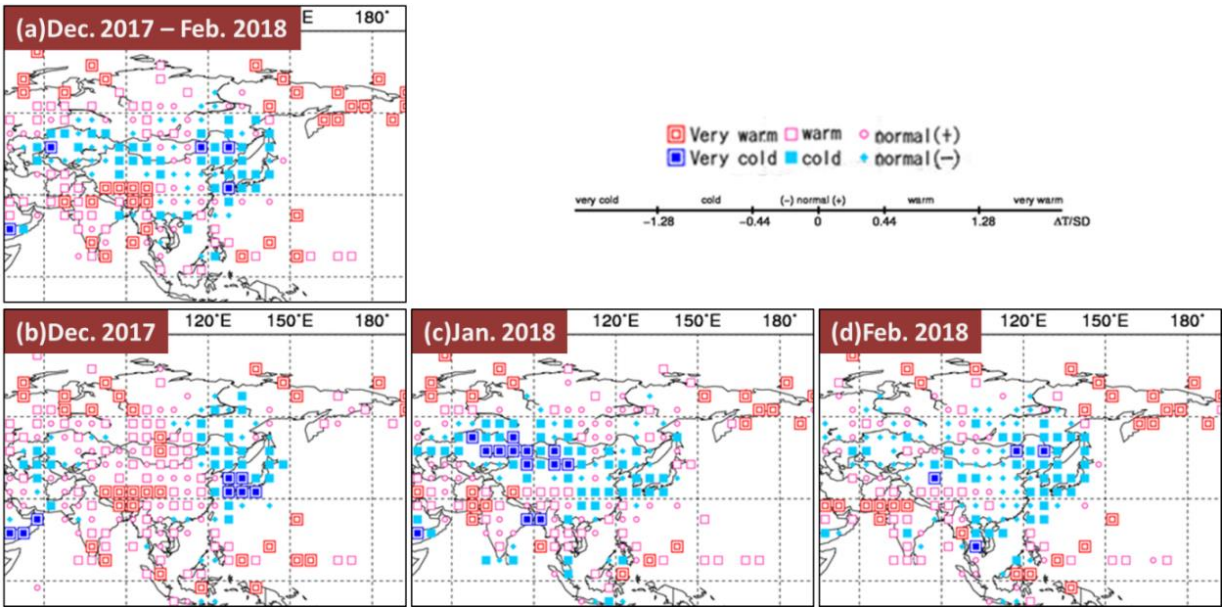

Figure 11 (a) Three-month mean temperature anomalies for December 2017 to February 2018, and monthly mean temperature anomalies for (b) December 2017, (c) January 2018 and (d) February 2018
Categories are defined by the three-month/monthly mean temperature anomaly against the normal divided by its standard deviation and averaged in 5° × 5° grid boxes. The thresholds of each category are -1.28, -0.44, 0, +0.44 and +1.28. Standard deviations were calculated from 1981 - 2010 statistics. Areas over land without graphical marks are those where observation data are insufficient or where normal data are unavailable.

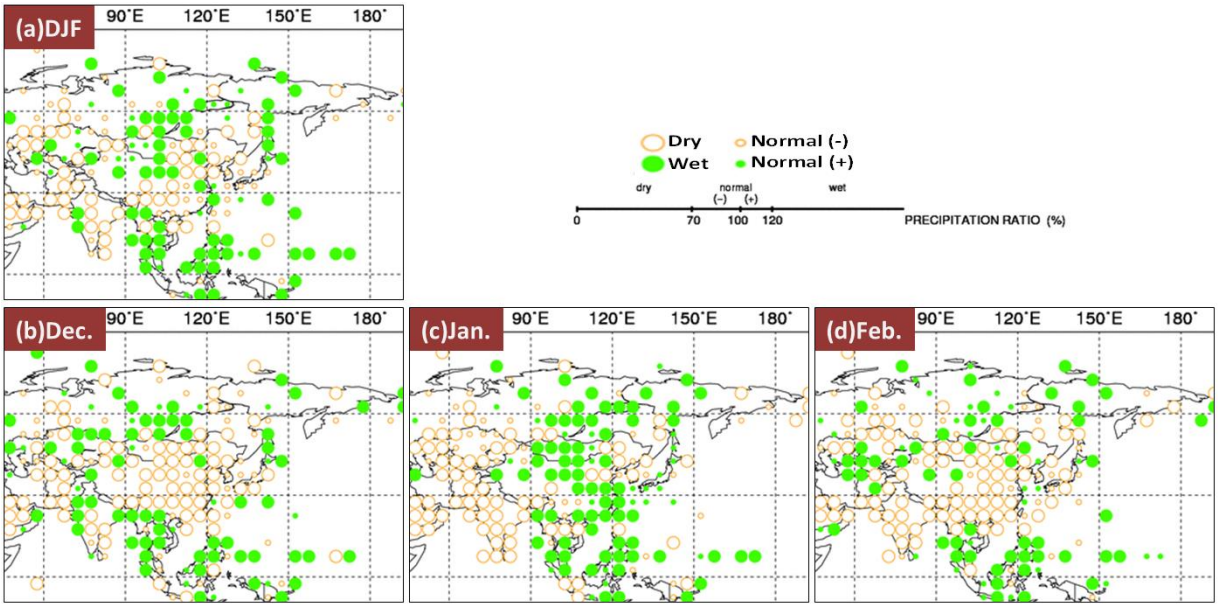

Figure 12 Three-month total precipitation ratio for December 2017 to February 2018, and monthly total precipitation ratio for (b) December 2017, (c) January 2018 and (d) February 2018
Categories are defined by the three-month mean precipitation ratio against the normal and averaged in 5° × 5° grid boxes. The thresholds of each category are 70, 100 and 120%. Areas over land without graphical marks are those where observation data are insufficient or where normal data are unavailable.

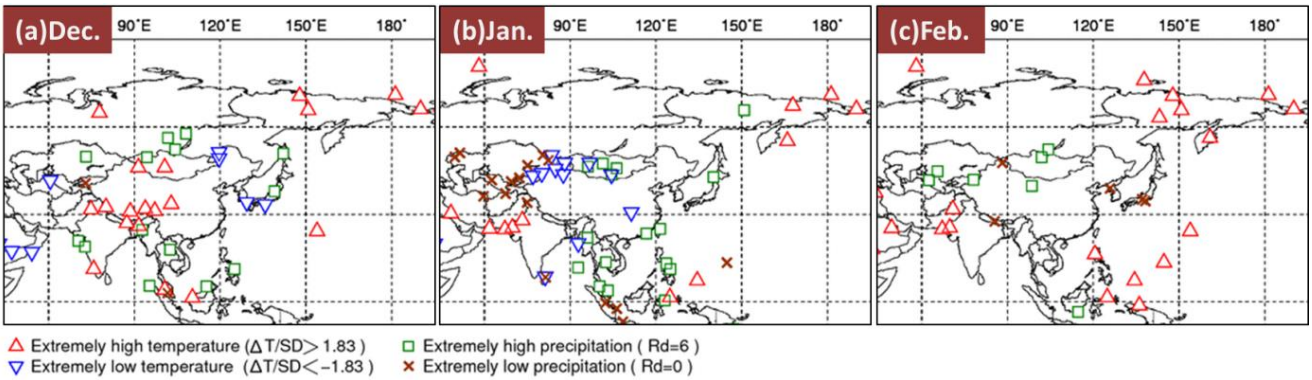

Figure 13 Extreme climate stations for (a) December 2017, (b) January 2018 and (c) February 2018
ΔT, SD and Rd indicate temperature anomaly, standard deviation and quintile, respectively.

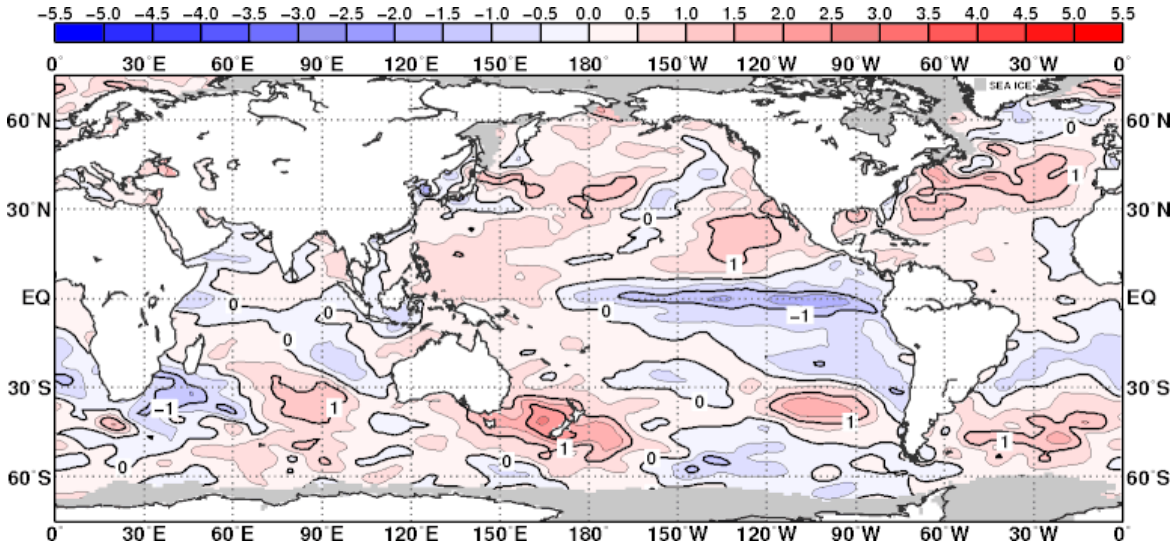

Figure 14 Three-month mean sea surface temperature (SST) anomalies for December 2017 to February 2018
The contour interval is 0.5˚C.

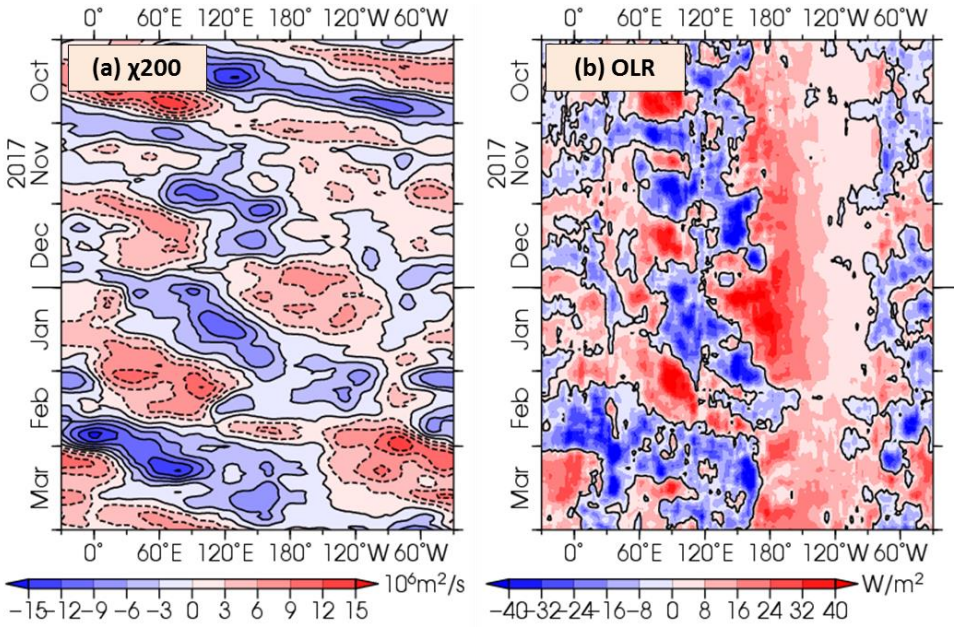

Figure 15 Time-longitude cross section of seven-day running mean (a) 200-hPa velocity potential anomalies, and (b) outgoing longwave radiation (OLR) anomalies around the equator (5°S – 5°N) for October 2017 to March 2018
(a) The blue and red shading indicates areas of divergence and convergence anomalies, respectively. (b) The blue and red shading indicates areas of enhanced and suppressed convective activity, respectively.

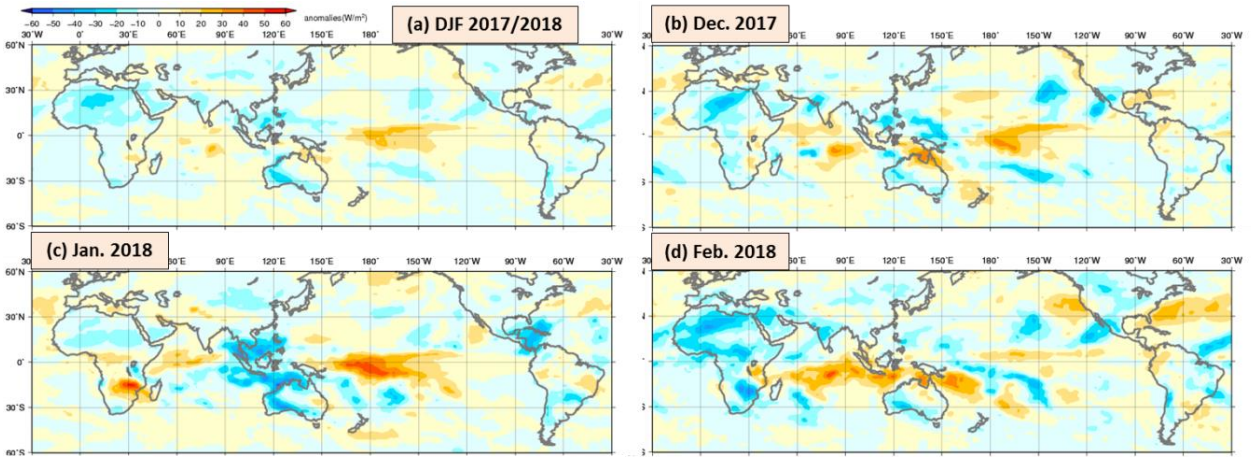

Figure 16 Outgoing longwave radiation (OLR) anomalies (a) averaged over the three months from December 2017 to February 2018, for (b) December 2017, (c) January 2018 and (d) February 2018
The blue and red shading indicates areas of enhanced and suppressed convective activity, respectively.

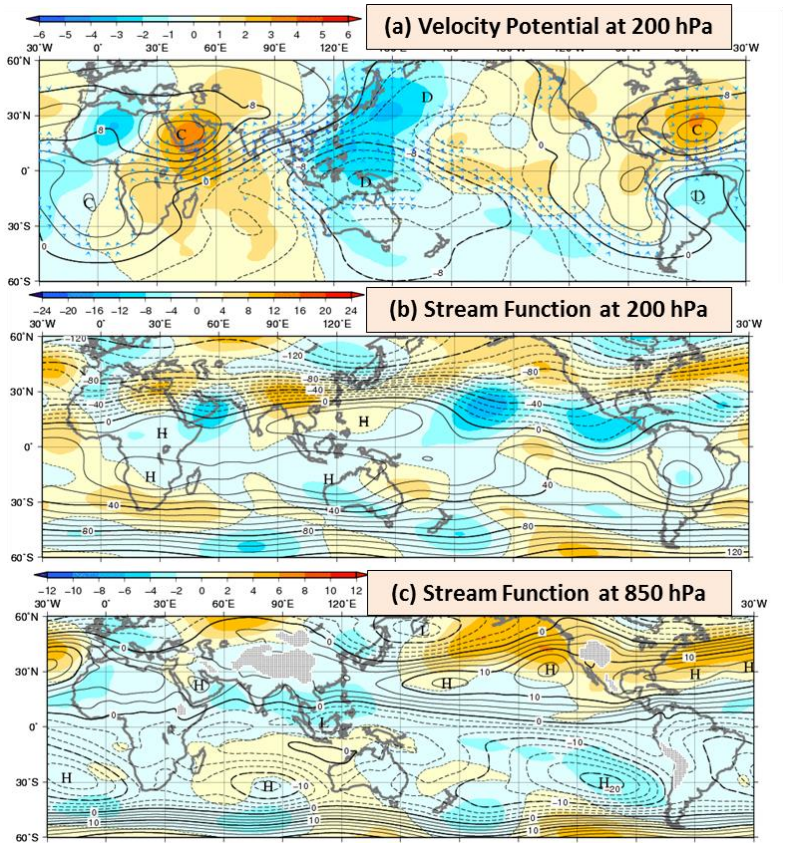

Figure 17 Three-month mean (a) 200-hPa velocity potential, (b) 200-hPa stream function, and (c) 850-hPa stream function for December 2017 to February 2018 (unit: 10^6 m^2/s)
(a) The contours indicate velocity potential at intervals of 2×10^6 m^2/s, and the shading shows velocity potential anomalies. D and C indicate the bottom and the peak of velocity potential, corresponding to the centers of large-scale divergence and convergence, respectively. (b, c) The contours indicate stream function at intervals of (b) 10 and (c) 2.5×10^6 m^2/s, and the shading shows stream function anomalies. H and L denote the centers of anticyclonic and cyclonic circulations, respectively.

2.2 Conditions in the extratropics

In the 500-hPa height field during winter 2017/2018 (Figure 18 (a)), the polar vortex in the Northern Hemisphere split into an Eastern Siberian part and a North American part in association with positive height anomalies over and around the North Pole. A clear wave train was observed over northern Eurasia, corresponding to the positive Eurasian (EU) teleconnection pattern (Wallace and Gutzler, 1982). The subtropical jet stream over Eurasia was displaced northward of its normal position in general while meandering northward over China and southward over Japan (Figure 19 (a)).

In the sea level pressure field (Figure 20 (a)), the Siberian High was stronger than normal in general. The Aleutian Low was shifted westward and was stronger than normal over and around the Kamchatka Peninsula. Temperatures at 850-hPa (Figure 21 (a)) were below normal over East Asia.

2.3 Primary factors contributing to the characteristics of the 2017/2018 Asian Winter Monsoon

Convective activity was enhanced over the Maritime Continent due to higher-than-normal SSTs in the tropical western Pacific region in association with the La Niña event observed from boreal autumn 2017 onward (Figure 14 and Figure 15 (a)). This enhanced convection strengthened the northwestward expansion of an upper-level high over the area from the South China Sea to the east of the Philippines (Figure 16 (a)), which in turn excited a Rossby wave, causing southward meandering of the subtropical jet stream around Japan (Figure 19 (a)).

The tropospheric polar vortex split in association with significant meandering of the polar-front jet stream over northern Eurasia caused by a blocking high over Western Siberia and other influences. One of the polar vortex sections shifted southward over Eastern Siberia (Figure 18 (a)), which caused southward meandering of the polar-front jet stream over the eastern part of East Asia.

Meandering of the subtropical and polar-front jet streams was also caused by Rossby wave packet propagation that can be traced back to the upper-level ridge over the North Atlantic (Figure 22).

As a result, northerly cold air flowed over the eastern part of East Asia more frequently than in normal winters, contributing to low temperatures in the region (Figure 11, Figure 21). There was a tendency for cold-air masses to flow over Japan, bringing intermittent heavy snowfall to some parts of the country.

(Hiroki Togawa, Climate Prediction Division)

References

Ishii, M., A. Shouji, S. Sugimoto and T. Matsumoto, 2005: Objective Analyses of Sea-Surface Temperature and Marine Meteorological Variables for the 20th Century using ICOADS and the Kobe Collection. Int. *J. Climatol.*, **25**, 865-879.

Kobayashi, S., Y. Ota, Y. Harada, A. Ebita, M. Moriya, H. Onoda, K. Onogi, H. Kamahori, C. Kobayashi, H. Endo, K. Miyaoka, and K. Takahashi, 2015: The JRA-55 Reanalysis: General Specifications and Basic Characteristics. *J. Meteorol. Soc.* Japan, **93**, 5 – 48.

Takaya, K., and H. Nakamura, 2001: A Formulation of a Phase-Independent Wave-Activity Flux for Stationary and Migratory Quasigeostrophic Eddies on a Zonally Varying Basic Flow. *J. Atmos. Sci.*, **58**, 608-627.

Wallace, J.M., and D.S. Gutzler, 1981: Teleconnections inthe Geopotential Height Field during the Northern Hemisphere Winter. *Mon. wea. Rev.*, **109**, 784-812.

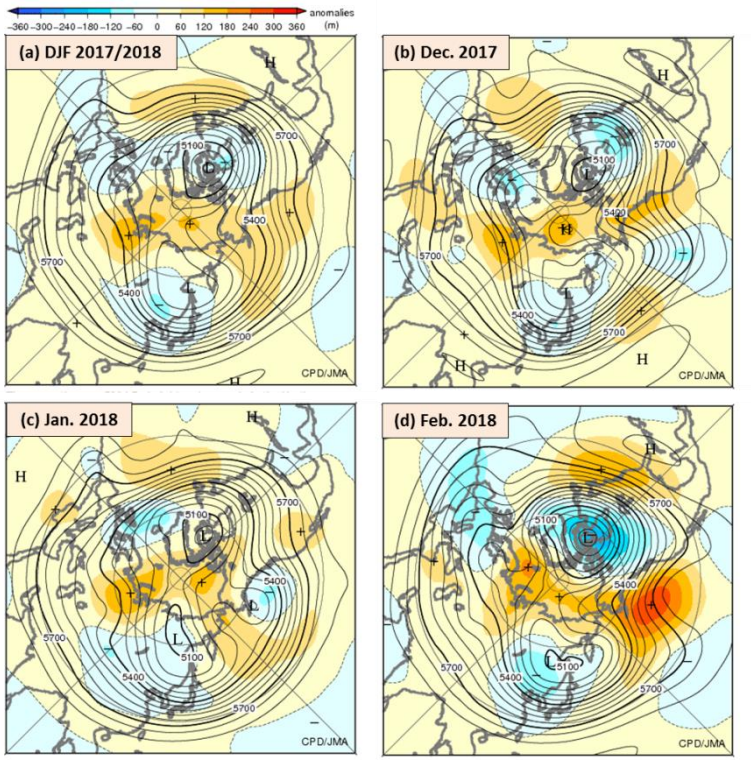

Figure 18 500-hPa height (a) averaged over the three months from December 2017 to February 2018, for (b) December 2017, (c) January 2018, and (d) February 2018
The contours indicate 500-hPa height at intervals of 60 m, and the shading denotes anomalies. H and L indicate the peak and bottom of 500-hPa height, respectively, and + (plus) and – (minus) show the peak and bottom of anomalies, respectively.

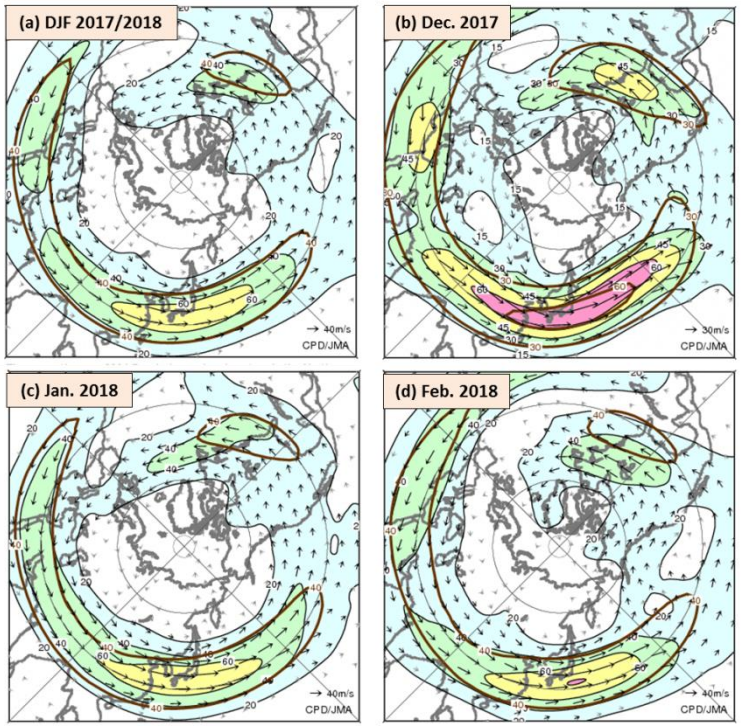

Figure 19 200-hPa wind speed and vectors (a) averaged over the three months from December 2017 to February 2018, for (b) December 2017, and (c) January 2018 and (d) February 2018

The black lines show wind speed at intervals of 20 m/s for (a), (c) and (d), and 15 m/s for (b). The brown lines show its normal at intervals of 40 m/s for (a), (c) and (d), and 30 m/s for (b). The base period for the normal is 1981 - 2010.

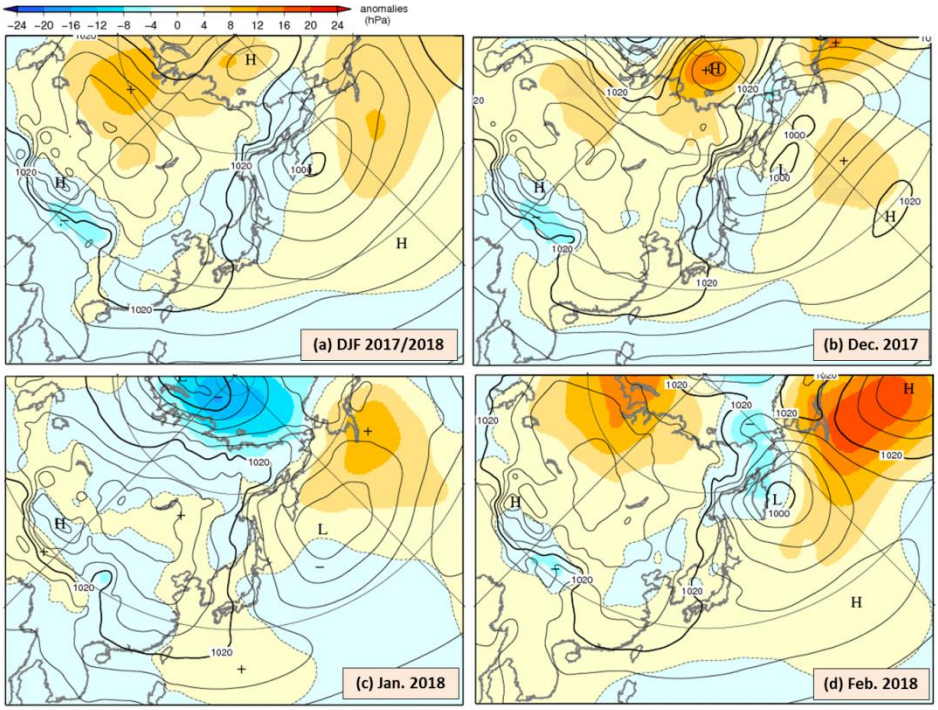

Figure 20 Sea level pressure (a) averaged over the three months from December 2017 to February 2018, for (b) December 2017, (c) January 2018 and (d) February 2018

The contours indicate sea level pressure at intervals of 4 hPa, and the shading shows related anomalies. H and L indicate the centers of high and low pressure systems, respectively, and + (plus) and – (minus) show the peak and bottom of sea level pressure anomalies, respectively.

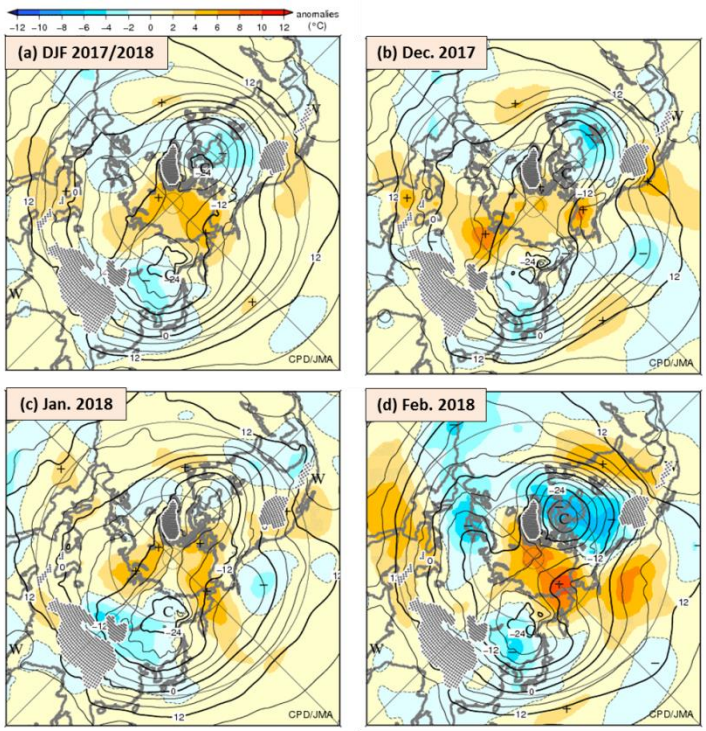

Figure 21 850-hPa temperature (a) averaged over the three months from December 2017 to February 2018, for (b) December 2017, (c) January 2018 and (d) February 2018

The contours indicate 850-hPa temperature at intervals of 4 °C and the shading shows related anomalies.

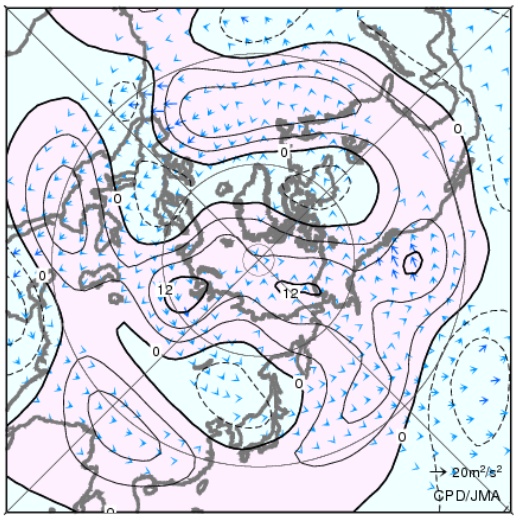

Figure 22 300-hPa stream function anomaly and wave activity flux averaged over the three months from December 2017 to February 2018

The counters indicate stream function anomalies at intervals of 4×10^6 m^2/s, and the vectors show wave activity flux (unit: m^2/s^2). The vectors are not shown where wave activity flux is less than 2 m^2/s^2. The wave activity flux was calculated with reference to Takaya and Nakamura (2001).